

# Supramolecular nesting of cyclic polymers

Dmitry V. Kondratuk,<sup>1</sup> Luís M. A. Perdigão,<sup>2</sup> Ayad M. S. Esmail,<sup>2</sup> James N. O'Shea,<sup>2</sup> Peter H. Beton<sup>2\*</sup> and Harry L. Anderson<sup>1\*</sup>

Advances in template-directed synthesis make it possible to create artificial molecules with protein-like dimensions, directly from simple components. These synthetic macromolecules have a proclivity for self-organisation, reminiscent of biopolymers. Here we report the synthesis of monodisperse cyclic porphyrin polymers, with diameters of up to 21 nm (750 C-C bonds). The ratio of the intrinsic viscosities for cyclic and linear topologies is 0.72, indicating that these polymers behave as almost ideal flexible chains in solution. When deposited on gold surfaces, the cyclic polymers display a new mode of two-dimensional supramolecular organisation, combining encapsulation and nesting: one nanoring adopts a near-circular conformation thus allowing a second nanoring to be captured within its perimeter, in a tightly folded conformation. Scanning tunnelling microscopy reveals that nesting occurs in combination with stacking when nanorings are deposited under vacuum, whereas when they are deposited directly from solution under ambient conditions, there is stacking or nesting, but not a combination of both.

The tertiary structures of biological macromolecules are achieved through folding, coiling and multiplex formation, driven by the cooperative effect of many weak interactions<sup>1</sup>. Synthetic monodisperse macromolecules with similar cooperative folding behaviour provide a viable approach to the programmed fabrication of 3D nanostructures<sup>2-5</sup>. Here we show that cyclic porphyrin polymers, with molecular weights of 30–60 kDa, self-assemble into nested structures on a gold surface. These nested assemblies are only observed when the cyclic polymer has 30 or more repeat units, in keeping with the predictions of a simple geometrical model.

The importance of non-covalent self-assembly in biology has inspired many studies of supramolecular organisation on surfaces<sup>6-8</sup>, generating 2D assemblies with progressively escalating complexity, from early work on simple structures such as clusters<sup>9</sup> and rows<sup>10,11</sup>, to nanoporous arrays<sup>12,13</sup>, host-guest architectures<sup>14-16</sup>, hierarchical arrangements<sup>17</sup>, and multicomponent assemblies<sup>17-19</sup>. However, cooperative conformational control has proved difficult to achieve, and this remains a significant gulf between artificial and biological systems. One reason for this difference is that biological macromolecules are much more flexible than the component molecules studied in 2D supramolecular assemblies which are small and, with some exceptions<sup>20,21</sup>, are often treated as quasi-rigid building blocks. Here we illustrate how interactions between large flexible molecules can result in biomimetic cooperative conformational organisation.

Studies of linear and cyclic butadiyne-linked zinc porphyrin oligomers (structures **L-PN<sub>THS</sub>** and **c-PN**, Fig. 1) have shown that the distance between the centres of the porphyrin units along the chain is  $a = 1.35 \text{ nm}$ <sup>5,22,23</sup>. Thus the contour length of a linear oligomer, or the perimeter of a nanoring, is  $Na$ , where  $N$  is the number of porphyrin repeat units. Previously we have shown that nanorings adsorbed on Au(111) exhibit flexibility<sup>24-26</sup>, and also that they can act as nanoscale traps for other adsorbed species, such as  $\text{C}_{60}$  guest molecules<sup>27</sup>. However, in order for one nanoring to be adsorbed inside another, the dimensions of the nanoring must

exceed a critical threshold. The footprint area of a nanoring is simply  $Nad$ , where  $d$  is the effective width of the chains (ca. 2.1 nm; see below). Note that this area is independent of conformation. The maximum area enclosed within the ring, and available for trapping a second nanoring, is  $\pi(Na/2\pi - d/2)^2$ . In order for self-trapping to occur, equation (1) must be satisfied,

$$\pi(Na/2\pi - d/2)^2 > Nad \quad (1)$$

which implies that the nanoring needs to consist of more than 29 porphyrin units ( $N \geq 29$ ).

The largest ring that we have synthesised previously is **c-P24** ( $N = 24$ )<sup>5</sup>. Here we describe how Vernier template-directed synthesis can be extended to prepare rings of up to 50 porphyrin units, and we show, using scanning tunnelling microscopy (STM), that rings with  $N \geq 30$  support a nested packing in which one nanoring is trapped in a compact conformation inside a second nanoring.

The synthesis of these very large macrocycles was achieved through a rational extension of Vernier-templating, by the cyclo-polymerisation of a linear porphyrin 10-mer **L-P10** in the presence of a 6-site template **T6** (favouring formation of the cyclic 30-mer, **c-P30**) or an 8-site template **T8** (favouring formation of the cyclic 40-mer, **c-P40**), as depicted in Fig. 1. In each case the expected Vernier product dominates the product distribution. These reactions are not completely selective, and cyclic polymers with 10, 20, 30, 40 and 50 porphyrin units can be isolated by recycling gel permeation chromatography (GPC). There has been much previous work on the synthesis of cyclic polymers<sup>28-32</sup>, but to the best of our knowledge, nanorings **c-P30**, **c-P40** and **c-P50** are the largest monodisperse covalent carbocyclic macrocycles yet reported. The 50-porphyrin nanoring **c-P50** contains an uninterrupted ring of 750 C-C bonds and has a diameter of 21 nm (molecular formula:  $\text{C}_{3400}\text{H}_{4100}\text{N}_{200}\text{O}_{200}\text{Zn}_{50}$ ). The largest previously reported synthetic macrocycle is a 32-porphyrin nanoring containing a cycle of 400 carbon atoms<sup>33</sup>. Höger and coworkers recently reported the synthesis of a molecular spoked wheel with a ring of 258 C-C bonds and a diameter of 12 nm<sup>34</sup>.

<sup>1</sup> Department of Chemistry, University of Oxford, Oxford OX1 3TA, UK. <sup>2</sup> School of Physics & Astronomy, University of Nottingham, Nottingham, NG7 2RD, UK. \*e-mail: harry.anderson@chem.ox.ac.uk, peter.beton@nottingham.ac.uk

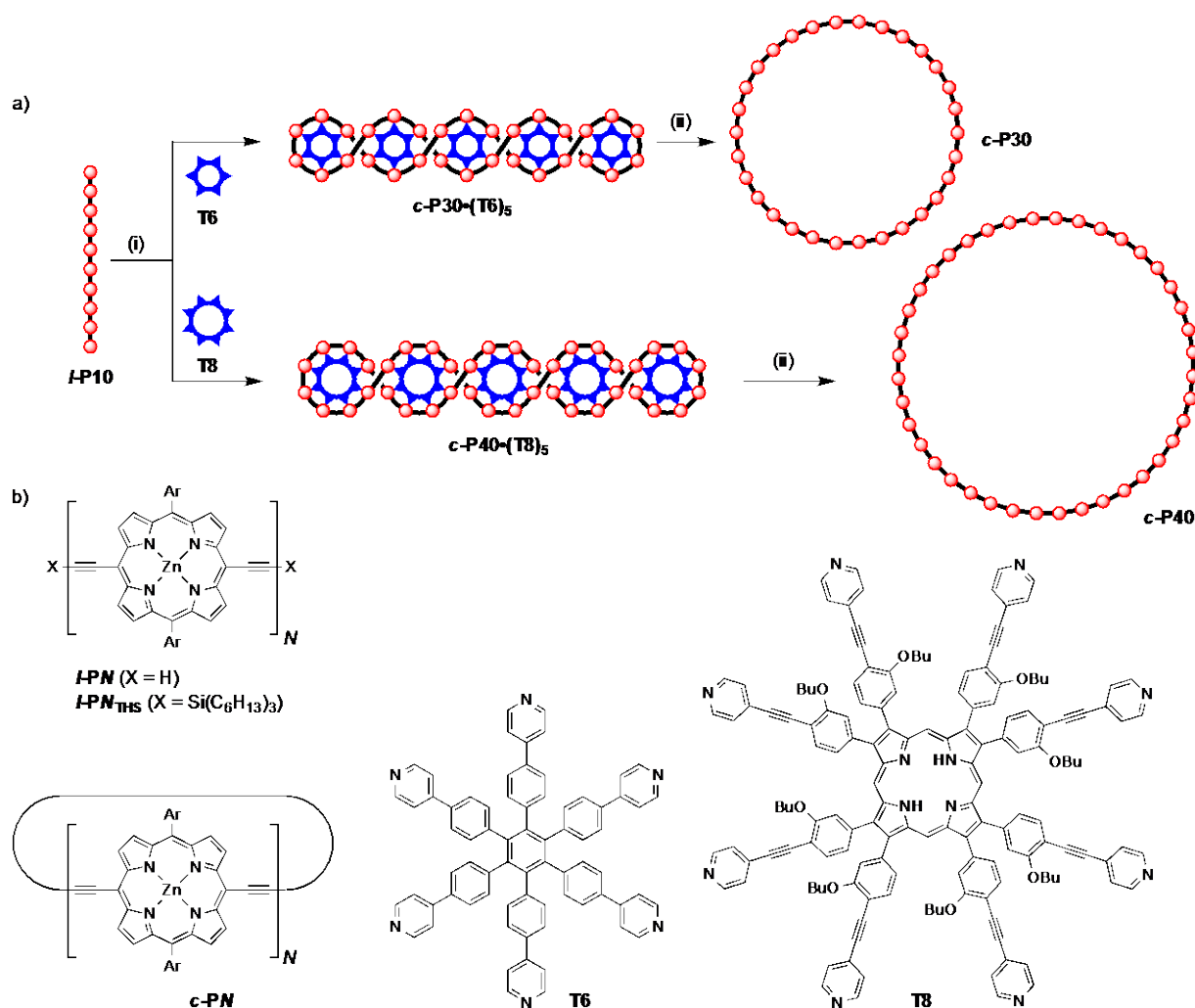


**Figure 1. Vernier template-directed synthesis of nanorings **c-P30** and **c-P40** and molecular structures of the components.** (a) Reaction scheme showing how the templates control the size of the final macrocycle. Reagents: i)  $PdCl_2(PPh_3)_2$ , CuI, benzoquinone,  $i$ -Pr<sub>2</sub>NH; ii) pyridine; (b) Structures of linear oligomers with terminal alkynes (**l-PN**) or terminal trihexylsilyl groups (**l-PN<sub>THS</sub>**), cyclic oligomers (**c-PN**), and templates (**T6** and **T8**). The solubilising sidechains on all the porphyrins are  $Ar = 3,5$ -bis(octyloxy)phenyl. THS stands for tri(*n*-hexyl)silyl.

## Results and discussion

**Synthesis.** We investigated the palladium-catalysed oxidative coupling of the linear zinc-porphyrin 10-mer **l-P10** in the presence of hexa-pyridyl template **T6**<sup>23,35</sup> and octa-pyridyl template **T8**<sup>36</sup> (Fig. 1). These reactions are expected to generate the nanoring-template complexes **c-P30•(T6)<sub>5</sub>** and **c-P40•(T8)<sub>5</sub>**, respectively, as mixtures of stereoisomers; the templates were displaced from the nanorings by addition of pyridine, prior to analysis and purification. Crude reaction mixtures were analysed by GPC and compared with the distribution of products from coupling under identical conditions in the absence of a template (Fig. 2). When no template is present, all the products are linear polymers; traces of linear oligomers **l-P10**, **l-P20** and **l-P30** can be detected but there is no evidence of cyclic products (Fig. 2a).

Coupling of **l-P10** in the presence of **T6** gives the expected cyclic porphyrin 30-mer **c-P30** as the main product (34% analytical yield, 26% isolated yield), however other by-products such as **c-P10**, **c-P20**, **c-P40** and **c-P50** are also formed (Fig. 2b). The reaction was

tested using a range of **l-P10** / **T6** ratios and the yield of **c-P30** was found to be highest (34% analytical yield) for a **l-P10** / **T6** ratio of 3/5. Reducing the amount of template below this stoichiometry increases the ratio of **c-P30** / **c-P10**, but reduces the yield of **c-P30** due to increased formation of linear polymers. Increasing the amount of template above 5/3 equivalents reduces the ratio **c-P30** / **c-P10** and reduces the yield of **c-P30**.

Changing the template to **T8** shifts the product-distribution to make **c-P40** predominate (36% analytical yield, 27% isolated yield), as expected from the Vernier principle (Fig. 2c). The yield of **c-P40** was found to be greatest for a **l-P10** / **T8** ratio of 1:1 (36% analytical yield). Reducing the amount of template below this stoichiometry increases the ratio of **c-P40** / **c-P10**, but reduces the yield of **c-P40** due to increased formation of linear polymers. Increasing the amount of template above 1 equivalent, reduces the ratio **c-P40** / **c-P10** and reduces the yield of **c-P40**.

The cyclic products, **c-P10**, **c-P20**, **c-P30**, **c-P40** and **c-P50**, were isolated by recycling GPC (see Supplementary Information). Their ring-sizes were

established by MALDI-TOF mass spectrometry and STM imaging (as discussed below), while their purities were confirmed by analytical GPC and  $^1\text{H}$  NMR spectroscopy.

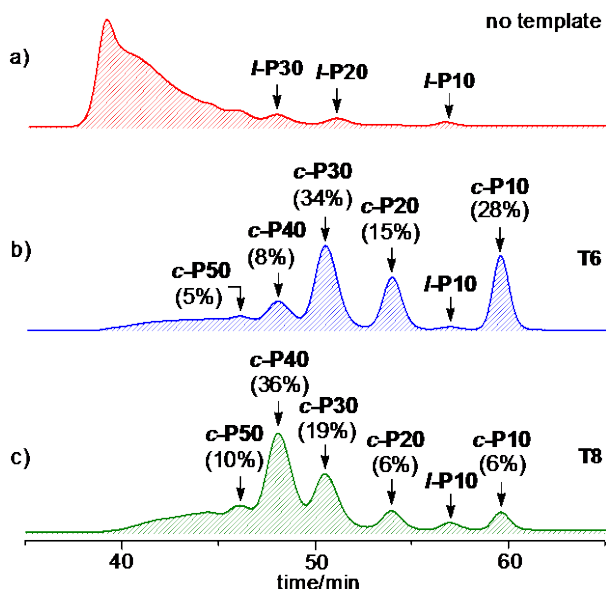


**Figure 2. Product distributions of coupling reactions.** Analytical GPC traces (toluene/1% pyridine, detection at 500 nm) of the crude reaction mixtures from coupling l-P10 (a) in the absence of a template, (b) in the presence of T6, and (c) in the presence of T8. The catalysts and 1,4-benzoquinone were removed by passing the sample through a short GPC column in  $\text{CHCl}_3$ /10% pyridine as eluent. The analytical yields were determined by comparison of resolved peaks in the corresponding recycling GPC traces (see Supplementary Information).

**Gel Permeation Chromatography.** All the isolated nanorings gave sharp single-component GPC profiles. The elution times confirm the molecular weights, when calibrated with data from previously characterised nanorings (c-P6, c-P8, c-P12, c-P16, c-P18 and c-P24), as shown from the plot of log molecular weight,  $\log M$ , vs. elution time  $t$  in Fig. 3. The points for linear and cyclic oligomers define two parallel straight lines, reflecting the more compact conformations of the cyclic oligomers. For molecular weights in the linear range for a GPC column, the elution time  $t$  is related to the molecular hydrodynamic volume  $V_h$  by equation 2<sup>37</sup>,

$$\log V_h = a - bt \quad (2)$$

where  $a$  and  $b$  are constants characteristic to the column. The hydrodynamic volume is related to the molecular weight  $M$  and the intrinsic viscosity  $[\eta]$  by equation 3 (where  $K$  is a constant)<sup>38</sup>.

$$V_h = KM[\eta] \quad (3)$$

Combining equations 2 and 3 gives:

$$\log M = a' - bt \quad (4)$$

where  $a' = (a - \log K - \log[\eta])$ . In Fig. 3, the data for cyclic and linear oligomers are fitted to two parallel straight lines, according to equation 4, giving  $a'_{\text{cyclic}} = 7.213 \pm 0.003$ ,  $a'_{\text{linear}} = 7.073 \pm 0.003$  and  $b = 0.053 \pm 0.001 \text{ min}^{-1}$ . If we assume that  $K$  is independent of the linear or cyclic topology of the polymer, then the ratio of

intrinsic viscosities for cyclic and linear chains of the same molecular weight is given by equation 5,

$$\Delta a' = a'_{\text{linear}} - a'_{\text{cyclic}} = \log([\eta]_{\text{cyclic}}/[\eta]_{\text{linear}}) \quad (5)$$

which gives  $[\eta]_{\text{cyclic}}/[\eta]_{\text{linear}} = 0.72 \pm 0.01$ . This ratio is close to the theoretical value of 0.66 for ideal flexible macromolecules in a theta solvent<sup>29,39</sup>, and to the values found experimentally for other linear and cyclic polymers ( $[\eta]_{\text{cyclic}}/[\eta]_{\text{linear}} = 0.6\text{--}0.7$ )<sup>29,40,41</sup>, indicating that the porphyrin polymers behave as flexible chains in solution.

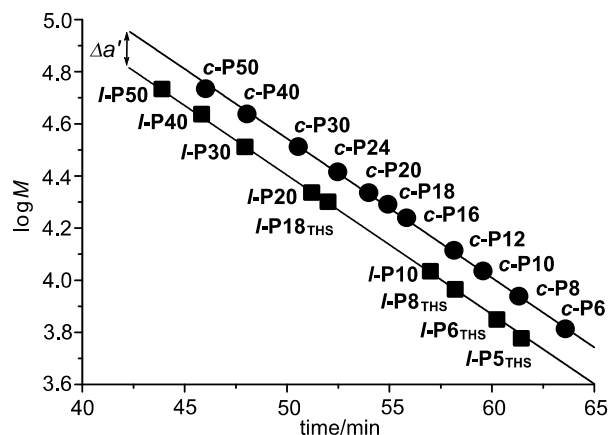


**Figure 3. GPC retention times of cyclic and linear porphyrin oligomers plotted against log molecular weight, showing that the rings are more compact than the linear chains.** Circles and squares indicate cyclic and linear oligomers, respectively. All data were recorded in toluene containing 1% pyridine to prevent aggregation. The points are fitted to two parallel lines, according to equation 4.

**Scanning Tunnelling Microscopy.** The cyclic structures of c-P10, c-P20, c-P30, c-P40 and c-P50 were confirmed using STM. Molecules were transferred from solution onto a Au(111) surface held under ultrahigh vacuum using electrospray deposition<sup>5,24,25</sup> and Fig. 4 shows STM images of each cyclic polymer. In common with our previous work<sup>5,25,26</sup> the nanorings are preferentially adsorbed in configurations overlapping, or partially overlapping, terrace steps on the Au(111) surface, and the porphyrin macrocycles lie parallel to the substrate. In many images it is possible to resolve the porphyrin units providing confirmation of the degree of polymerisation, simply by counting the bright contrast features around the perimeter of a nanoring. This numbering is included for the c-P30 and c-P40 nanorings in Fig. 4 (further images, including those acquired for larger areas are included in the Supplementary Information (SI)).

We also observe stacking of c-P30, c-P40 and c-P50 nanorings, with two or three nanorings lying directly above each other, in an eclipsed geometry, as reported recently for c-P24<sup>26</sup>. These assemblies can be identified from their topographic height (~0.4 nm for double stacks, ~0.7 nm for triple stacks) in contrast to the single-height rings (height ~0.1 nm) observed for c-P20 and c-P10 (see height profiles in SI).

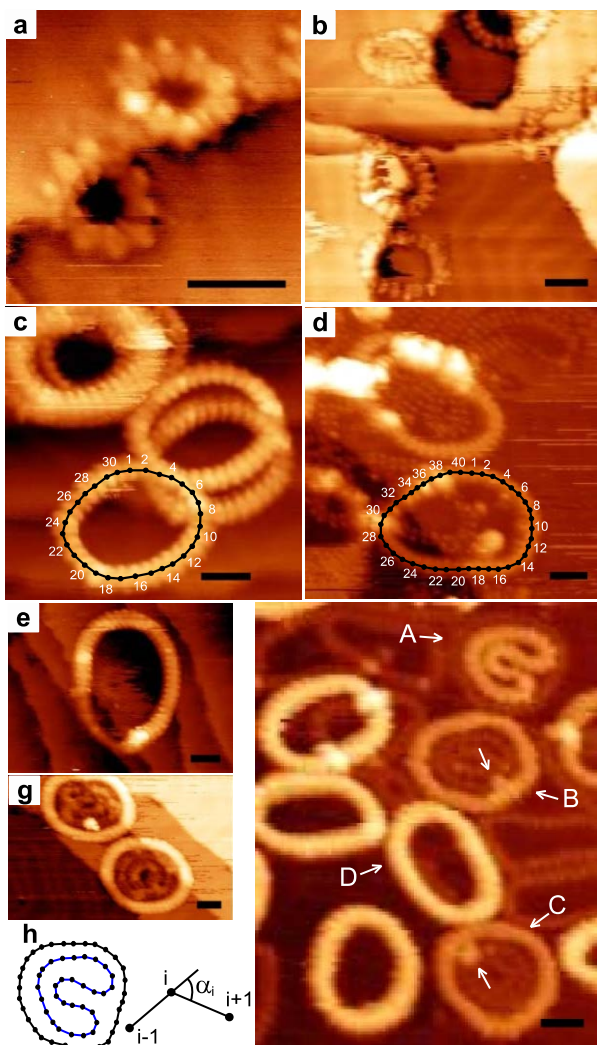


**Figure 4.** STM images of nanorings deposited on gold surfaces under UHV. (a) *c*-P10. (b) *c*-P20. (c) *c*-P30. (d) *c*-P40. (e) *c*-P50. (f) Nested nanoring complexes of *c*-P30; A is a “double-in-single” nested structure consisting of two stacked folded rings inside a single open ring; B and C are nested “single-in-double” structures consisting of a single folded ring inside a two-layer stack of open rings; D is a triple-stack nanoring. (g) Nested nanoring complexes of *c*-P40 consisting of single-height inner rings within double-height outer rings; (h) Schematic of the nested *c*-P30 structure A and the definition of the angle,  $\alpha_i$ . Selected rings in images (c) and (d) have numbering of the subunits included. The arrows identify bright features on the inner nanoring discussed in text. All scale bars are 5 nm; scanning parameters are included in SI.

The nested self-trapped supramolecular arrangement is observed for nanorings with 30 and 40 porphyrin groups. In Fig. 4f, we show a zoomed image of *c*-P30; in the top right corner a tightly packed nanoring with bright contrast is enclosed within a lower contrast near-circular nanoring (marked A). The contrast levels correspond to different topographic heights and we identify the higher contrast interior structure as a stack of two nanorings, while the outer near-circular conformation is a single-height nanoring. There are two other nested structures in this image (marked B and C) in which the overall conformation of the inner and outer nanorings are very similar to structure A, but the relative contrast of the inner

and outer nanorings is reversed. Thus B and C are both formed from a single-height nanoring enclosed within a near-circular stack of two nanorings. Similarly, the nested *c*-P40 structures shown in Fig. 4g, have single-height inner rings within double-height outer rings. In Fig. 4f there are also several non-nested structures with brighter contrast which we identify, from their topographic height as stacks of three nanorings (for example D).

**Table 1 | Distribution of nanorings in identifiable nested, non-nested and open stacked structures from electrospray deposition under UHV.<sup>a</sup>**

	Nanorings in nested structures			Nanorings in open non-nested structures		
	1-in-1	1-in-2	2-in-1	single	2-stack	3-stack
<i>c</i> -P30	1.0%	9%	1.5%	7%	16%	65.5%
<i>c</i> -P40	1.0%	22.5%	1.5%	3%	20%	52%

<sup>a</sup> Statistics based on STM images of 522 *c*-P40 nanorings and 320 *c*-P30 nanorings, of which 324 and 119, respectively, were in overlapping disordered structures and are not included here; 1-in-1, 1-in-2 and 2-in-1 denote single-in-single, single-in-double and double-in-single nested structures. The overall fraction of nanorings in nested structures is higher for *c*-P40 (25%) than for *c*-P30 (11.5%); the single-in-double is observed much more frequently than the double-in-single structure.

The fraction of *c*-P30 and *c*-P40 in various nested and non-nested geometries is analysed in Table 1, showing that the single-in-double is by far the most common nested structure.

The conformation of the compact nested nanoring is most clearly resolved for nanoring A where a series of three ‘hairpin’ bends through  $\sim 180^\circ$  deform the nanoring into a ‘C’ shape. The separation between porphyrin groups on neighbouring polymers is  $d = 2.1 \pm 0.1$  nm in regions where the curvature is small (for example the boundary between single-height nanorings slightly above the letter C in Fig. 4f), close to the separation measured for linear oligomers (see SI); this value is used in our estimate of the minimum size for nesting in the introduction. However, the separation of porphyrin groups in the inner and outer nanorings forming the nested structure can deviate from this value. In particular, the separation measured for structure A is in the range 1.6–1.8 nm in regions where the curvature of the inner nanoring is highest, i.e. close to the hairpin bends.

It is possible to map the porphyrin positions in the nested structure A, (see schematic in Fig. 4h), from which we estimate the elastic energy required to form the nested conformation. Approximating the shape to 30 segments with an angle  $\alpha_i$  between the  $i$ th and  $(i+1)$ th segments (see Fig. 4h) we estimate,

$$E_B = \frac{\kappa_B}{2a} \sum_{i=1}^N \alpha_i^2 \quad (6)$$

where  $\kappa_B$  is the bending coefficient, estimated previously to be 0.07 and 0.03 nN nm<sup>2</sup> for double and single layer nanorings respectively<sup>24</sup>. Accordingly we estimate  $E_B \approx 2.6$  eV for the nested double-height nanoring in Fig. 4f. Note that this energy, though large, is distributed over 60 porphyrin-butadiene groups.

In considering the overall energy difference between a nested double/single-stacked nanoring and triply stacked structure, we note that there is a gain in adsorption energy arising from the interaction of an additional nanoring with the gold surface. This must be greater than the energy



required to elastically deform a coiled nanoring in order for the nested structure to be stable. The typical adsorption energies of porphyrins on Au(111) are in the range 2–4 eV; for example the adsorption energy of tetraphenylporphyrin on Au(111) has been calculated<sup>42</sup> to be 3.3 eV. Since the overall adsorption energy would scale with  $N$ , this would result in an adsorption energy of  $\sim 100$  eV for **c-P30**, much greater than the bending energy estimated above. For these large molecules which are composed of 4770 atoms high-level calculations of adsorption energies are not currently possible, but this order of magnitude argument illustrates that if there is a conformation available which can accommodate a nested structure, we would expect it to be energetically stable.

In previous work on **c-P24**, we showed that the stacking is related to the choice of solvent<sup>26</sup> (in particular it is suppressed through the addition of pyridine to the electrospray solution). To determine whether the nesting, and its combination with stacking, is also solvent-dependent we have investigated layers formed by immersion under ambient conditions using a flame-annealed Au(111) thin film on mica as a substrate. STM images were then acquired under ambient conditions (see Methods and SI). When samples are deposited from methanol/toluene (5:3 volume ratio; 12.5  $\mu\text{g/mL}$  of **c-P30**) we see many bright nanorings with lateral dimensions  $\sim 13$  nm, close to the value expected for **c-P30** (Fig. 5a). Many of the nanorings are slightly distorted from a circular shape and there are regions where partially-ordered nanorings form a quasi-close packed hexagonal arrangement. A histogram of the heights of the nanorings in this image (Fig. 5b) shows a clear peak around 0.7 nm corresponding to a height of three stacked nanorings.

In contrast, deposition from a solution of **c-P30** (12.5  $\mu\text{g/mL}$ ) in toluene (which is not compatible with electrospray) shows very few stacked nanorings (Fig. 5c). Under these conditions, we see single-height rings with a highly non-circular shape which form a disordered arrangement (Fig. 5e). A histogram (Fig. 5d) shows a clear peak at a height of  $\sim 0.1$  nm confirming the predominance of single-height structures. These results confirm the dominant role of solvent in the stacking, and demonstrate that this effect is not limited to electrospray deposition.

For the surfaces prepared from methanol:toluene (5:3), we do not observe any nested structures (see Fig. 5a,b) and the triple-height stacks are stable under STM imaging. The majority of nanorings ( $> 90\%$ ) are incorporated as the near-circular triple height stacks discussed above, with the remainder in less ordered, in many cases overlapping, structures. Thus, stacking occurs for both solution and electrospray deposition, but the combination of stacking and nesting is only observed using electrospray. This implies that the stacks are pre-formed in the methanol:toluene solution consistent with previous work. However, the nesting observed using methanol:toluene depends on the method of deposition, and it therefore probably occurs on adsorption rather than in solution. Noting that in almost all cases the nesting observed for electrospray deposition involves double-in-single, or single-in-double structures, we propose that these arrangements originate from triple stacks of

nanorings which are formed in solution and then relax through rearrangement when they impinge on the surface. In the light of this discussion, we also interpret many of the complex structures of overlapping nanorings, for example in Fig. 4c, as multiple (commonly triple) stacks which impinge on the substrate in electrospray deposition and partially collapse into slipped stacks or nested arrangements. In contrast, there are far fewer partially collapsed structures on solution deposition from methanol/toluene (Fig. 5a); stacking is retained under these conditions.

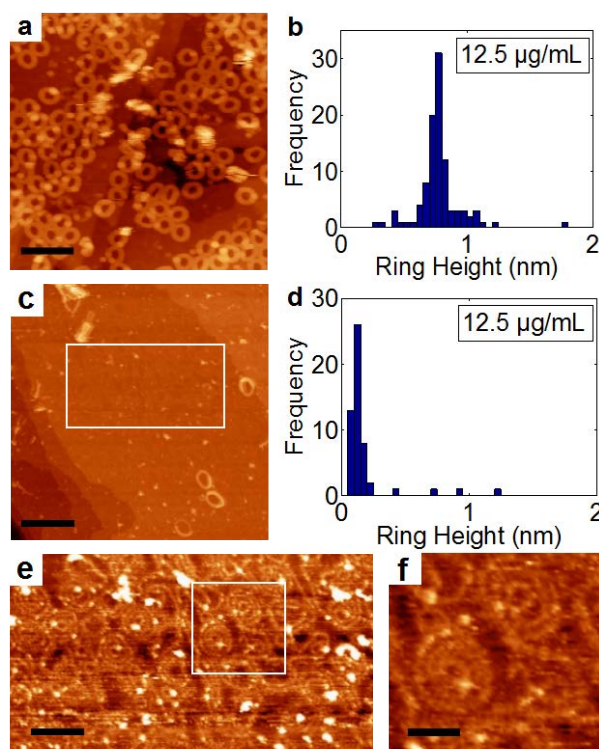


**Figure 5. STM images of **c-P30** deposited on Au(111) from solution and imaged under ambient conditions.** (a) Stacked nanorings deposited from a methanol:toluene mixture (5:3 v/v); (b) histogram of heights showing triple stacked nanorings. (c) Single-height nanorings deposited from toluene; (d) histogram of heights showing a peak at  $\sim 0.1$  nm corresponding to single-height nanorings. (e) Zoomed image of highlighted area in (c) showing disordered arrangement of single-height **c-P30**; (f) further zoom of highlighted area in (e) showing nested structures. All samples were deposited from a solution of **c-P30** of concentration 12.5  $\mu\text{g/mL}$ . Scale bars: (a) 36 nm; (c) 36 nm (e) 18 nm; (f) 8 nm.

We now consider whether stacking is required as a precursor to the formation of the nested arrangement. This is addressed in Fig. 5c-f which shows the surface after deposition from toluene. Under these conditions stacking is almost completely suppressed and we observe a disordered array of single-height nanorings (Fig. 5e). Importantly, the bending coefficient of single height rings is much lower (by a factor 3) than that of triple stacks, and so they are much more flexible resulting in a highly-deformed non-circular conformation. Nested structures are observed under these conditions (Fig. 5f) and our images show that the enclosed nanorings have a similar conformation of three hairpin bends to that observed for

electrospray deposition under UHV. However, a significant difference is that for solution-phase deposition, we only observe nested structures in which both the inner and outer nanoring are single-height. The absence of any combinations of double- and single-height nesting, similar to those observed for electrospray conditions, provides further evidence that the formation of such structures requires solvent-induced stacking as proposed above. We typically observe ~8 single-in-single nested structures in a 100 nm × 100 nm image on surfaces such as that shown in Fig. 5e, and ~10% of the surface is covered with nanorings adsorbed in nested arrangements. However, due to the flexibility of the single height nanorings there are no clear examples of near-circular ‘empty’ nanorings which might accommodate a coiled nested structure; the only nanorings which have a near-circular conformation in Fig. 5e serve as the outer ring of a nested structure.

As we show above in equation (1), a simple argument leads to a critical value of  $N \approx 29$  for which nesting would be sterically permitted, consistent with our observations (and also the absence of nesting for  $N = 24$ , the next smallest nanoring synthesised to date). However, the available area in the **c-P30** nested structures is less than the maximum assumed in deriving this simple rule since the outer nanoring is not perfectly circular. Interestingly, although the single-height nested nanorings, **B** and **C**, have a conformation which, overall, is very similar to the double-height nested ring, there are also bright features identified by arrows in Fig. 4f. We attribute these features to small sections where the nested nanoring adopts a conformation where, locally, the porphyrin groups are either non-parallel to the substrate, or there is a region of self-overlapping; this may be a route to accommodate the single nanoring in a nested structure even for cases where the available area is marginally lower than the critical size estimated above.

## Conclusion

We have shown that Vernier-template directed synthesis can be extended to provide access to large cyclic polymers. The porphyrin nanorings **c-P30**, **c-P40** and **c-P50** are the largest monodisperse covalent synthetic macrocycles yet reported, with carbocyclic topologies of up to 750 C-C bonds. These cyclic polymers are highly amenable for imaging by STM, both under UHV, when deposited by electrospray, and under ambient conditions, deposited from solution. These STM experiments reveal that the larger rings, with 30 or more repeat units, form nested complexes, with one nanoring molecule folded inside another circular nanoring. Supramolecular nesting was observed under both UHV and solution-phase conditions. Under UHV, nesting is frequently combined with stacking, so that a stack of folded molecules sits inside a single-height extended ring, or such that a single folded molecule sits inside a stack of two extended ring molecules. The statistical distribution of these stacked/nested assemblies strongly suggests that they are formed, under UHV electrospray conditions, by the on-surface rearrangement of triple-decker nanoring stacks. This work illustrates the tendency for large macrocyclic molecules to undergo biomimetic self-assembly, and the power of STM for probing supramolecular processes.

## Methods

**Vernier-templated polymerisation of *l*-P10 in the presence of T6.** The template **T6** (0.68 mg, 0.68  $\mu$ mol) and the linear porphyrin 10-mer ***l*-P10** (4.7 mg, 0.41  $\mu$ mol) were dissolved in  $\text{CHCl}_3$  (5.0 mL) and heated at 50 °C until clear solution formed. A catalyst solution was prepared by dissolving  $\text{Pd}(\text{PPh}_3)_2\text{Cl}_2$  (1.0 mg, 1.4  $\mu$ mol),  $\text{CuI}$  (1.2 mg, 6.9  $\mu$ mol) and 1,4-benzoquinone (3.0 mg, 28  $\mu$ mol) in  $\text{CHCl}_3$  (700  $\mu$ L) and *i*-Pr<sub>2</sub>NH (60  $\mu$ L). 250  $\mu$ L of the catalysts solution was added to a solution of ***l*-P10** and **T6** at 0 °C and then stirred at 0 °C for 2 hours and then at 20 °C for 12 hours. The porphyrin oligomers mixture was separated from the catalysts by size-exclusion chromatography (Biobeads SX-1,  $\text{CHCl}_3$ /10% pyridine) and further separated by recycling gel permeation chromatography to yield **c-P10** (1.2 mg, 26%), **c-P20** (0.8 mg, 17%), **c-P30** (1.2 mg, 26%) and **c-P40** (0.5 mg, 11%).

**Scanning tunnelling microscopy:** (i) UHV experiments - a solution of **c-P10**, **c-P20**, **c-P30**, **c-P40** or **c-P50** in toluene-methanol (3:1 by volume; concentration, 100  $\mu\text{g mL}^{-1}$ ) was deposited on the substrate (gold on mica) by electrospray. Images were acquired in ultrahigh vacuum using electrochemically etched tungsten tips, in constant-current mode at room temperature; (ii) the samples in Fig. 5 were prepared by immersing a gold on mica substrate in a solution for 10 minutes. Further details are included in the SI.

## References

- Hunter, C. A. & Anderson, H. L. What is cooperativity? *Angew. Chem. Int. Ed.* **48**, 7488–7499 (2009).
- Cheng, R. P. Beyond de novo protein design – de novo design of non-natural folded oligomers. *Curr. Opin. Struc. Biol.* **14**, 512–520 (2004).
- Gan, Q., et al. Helix-rod host-guest complexes with shuttling rates much faster than disassembly. *Science* **331**, 1172–1175 (2011).
- Sakai, N., Mareda, J. & Matile, S. Artificial  $\beta$ -barrels. *Acc. Chem. Res.* **41**, 1354–1365 (2008).
- Kondratuk, D. V., et al. Two Vernier-templated routes to a 24-porphyrin nanoring. *Angew. Chem. Int. Ed.* **51**, 6696–6699 (2012).
- Bartels, L. Tailoring molecular layers at metal surfaces. *Nature Chem.* **2**, 87–95 (2010).
- Kudernac, T., Lei, S., Elemans, J. A. A. W. & De Feyter, S. Two-dimensional supramolecular self-assembly: nanoporous networks on surfaces. *Chem. Soc. Rev.* **38**, 402–421 (2009).
- Barth, J. V, Costantini, G. & Kern, K. Engineering atomic and molecular nanostructures at surfaces. *Nature* **437**, 671–679 (2005).
- Böhringer, M. et al. Two-dimensional self-assembly of supramolecular clusters and chains. *Phys. Rev. Lett.* **1**, 324–327 (1999).
- Yokoyama, T., Yokoyama, S., Kamikado, T., Okuno, Y. & Mashiko, S. Selective assembly on a surface of supramolecular aggregates with controlled size and shape. *Nature* **413**, 619–621 (2001).
- Barth, J. V et al. Building supramolecular nanostructures at surfaces by hydrogen bonding. *Angew. Chem. Int. Ed.* **39**, 1230–1234 (2000).
- Griessl, S., Lackinger, M., Edelwirth, M., Hietschold, M. & Heckl, W. M. Self-assembled two-dimensional molecular host-guest architectures from trimesic acid. *Single Mol.* **3**, 25–31 (2002).
- Theobald, J. A., Oxtoby, N. S., Phillips, M. A., Champness, N. R. & Beton, P. H. Controlling molecular deposition and layer structure with supramolecular surface assemblies. *Nature* **424**, 1029–1031 (2003).
- Stepanow, S. et al. Steering molecular organization and host-guest interactions using two-dimensional nanoporous coordination systems. *Nat. Mater.* **3**, 229–2233 (2004).

15. Griessl, S. J. H. *et al.* Incorporation and manipulation of coronene in an organic template structure. *Langmuir* **20**, 9403–9407 (2004).
16. Blunt, M. O. *et al.* Guest-induced growth of a surface-based supramolecular bilayer. *Nature Chem.* **3**, 74–78 (2011).
17. Spillmann, H. *et al.* Hierarchical assembly of two-dimensional homochiral nanocavity arrays. *J. Am. Chem. Soc.* **125**, 10725–8 (2003).
18. Furukawa, S. *et al.* Structural transformation of a two-dimensional molecular network in response to selective guest inclusion. *Angew. Chem. Int. Ed.* **46**, 2831–2834 (2007).
19. Nath, K. G. *et al.* Rational modulation of the periodicity in linear hydrogen-bonded assemblies of trimesic acid on surfaces. *J. Am. Chem. Soc.* **128**, 4212–4213 (2006).
20. Klappenberger, F. *et al.* Conformational adaptation in supramolecular assembly on surfaces. *ChemPhysChem* **8**, 1782–1786 (2007).
21. Jung, T. A., Schlittler, R. R. & Gimzewski, J. K. Conformational identification of individual adsorbed molecules with the STM. *Nature* **386**, 696–698 (1997).
22. Taylor, P. N., Huuskonen, J., Rumbles, G., Aplin, R. T., Williams, E. & Anderson, H. L. Conjugated porphyrin oligomers from monomer to hexamer. *Chem. Commun.* 909–910 (1998).
23. Sprafke, J. K. *et al.* Belt-shaped  $\pi$ -systems: relating geometry to electronic structure in a six-porphyrin nanoring. *J. Am. Chem. Soc.* **133**, 17262–17273 (2011).
24. Saywell, A., *et al.* Conformation and packing of porphyrin polymer chains deposited using electrospray on a gold surface. *Angew. Chem. Int. Ed.* **49**, 9136–9139 (2010).
25. O'Sullivan, M. C., *et al.* Vernier templating and synthesis of a 12-porphyrin nanoring. *Nature* **469**, 72–75 (2011).
26. Svatek, S. A., *et al.* Mechanical stiffening of porphyrin nanorings through supramolecular columnar stacking. *Nano Lett.* **13**, 3391–3395 (2013).
27. Wieland, M. B. *et al.* Height dependent molecular trapping in stacked cyclic porphyrin nanorings. *Chem. Commun.* **50**, 7332–7335 (2014).
28. Bielawski, C. & Grubbs, R. H. Living ring-opening metathesis polymerization. *Prog. Pol. Sci.* **32**, 1–29 (2007).
29. Semlyen, J. A., “Cyclic Polymers”, Kluwer Academic, 2<sup>nd</sup> ed. (2000).
30. Jia, Z. & Monteiro, M. J. Cyclic polymers: methods and strategies. *J. Polym. Sci. Pol. Chem.* **50**, 2085–2097 (2012).
31. Mayor, M. & Didschies, C. A giant conjugated molecular ring. *Angew. Chem. Int. Ed.* **42**, 3176–3179 (2003).
32. Aggarwal, A. V. *et al.* Fluctuating exciton localizations in giant  $\pi$ -conjugated spoked-wheel macrocycles. *Nature Chem.* **5**, 964–970 (2013).
33. Hori, T., *et al.* Synthesis of nanometer-scale porphyrin wheels of variable size. *Chem. Eur. J.* **14**, 582–595 (2008).
34. May, R., Jester, S., Höger, S. A giant molecular spoked wheel. *J. Am. Chem. Soc.* **136**, 16732–16735 (2014).
35. Hoffmann, M., *et al.* Enhanced  $\pi$ -conjugation around a porphyrin [6]nanoring. *Angew. Chem. Int. Ed.* **47**, 4993–4996 (2008).
36. Hoffmann, M., Wilson, C. J., Odell, B. & Anderson H. L. Template-directed synthesis of a  $\pi$ -conjugated porphyrin nanoring. *Angew. Chem. Int. Ed.* **46**, 3122–3125 (2007).
37. Mahabadi, H. K. & Rudin, A. Effect of solvent on concentration dependence of hydrodynamic volumes and GPC elution volumes. *Polym. J.* **11**, 123–131 (1979).
38. Grubisic, Z., Rempp, P. & Benoit, H. A universal calibration for gel permeation chromatography. *J. Polym. Sci. Pol. Lett.* **5**, 753–759 (1967).
39. Fukatsu, M. & Kurata, M. Hydrodynamic properties of flexible ring macromolecules. *J. Chem. Phys.* **44**, 4539–4545 (1966).
40. Dodgson, K. & Semlyen, J. A. Studies of cyclic and linear poly(dimethylsiloxanes): 1. Limiting viscosity number-molecular weight relationships. *Polymer* **18**, 1265–1268 (1977).
41. Kricheldorf, H. R. Cyclic polymers: synthetic strategies and physical properties. *J. Polym. Sci. Pol. Chem.* **48**, 251–284 (2010).
42. Brede, J. *et al.* Dynamics of molecular self-ordering in tetraphenyl porphyrin monolayer on metallic substrates. *Nanotechnology* **20**, 275602 (2009).

## Acknowledgements

We thank the Engineering and Physical Sciences Research Council (EPSRC), the European Research Council (ERC) and the Clarendon Fund for support, and the EPSRC mass spectrometry service (Swansea) for mass spectra.

## Author contributions

H.L.A. and D.V.K. designed the synthesis of cyclic polymers. P.H.B., L.M.A.P., J.N.O.S. and A.M.S.E. developed the protocols required for STM imaging. Synthesis and solution-phase characterisation were carried out by D.V.K. UHV and ambient STM experiments were carried out by L.M.A.P. and A.M.S.E. respectively. The manuscript was written by D.V.K., H.L.A. and P.H.B. All authors contributed towards data analysis and edited the manuscript.

## Additional information

The authors declare no competing financial interests. Supplementary information accompanies this paper at [www.nature.com/naturechemistry](http://www.nature.com/naturechemistry). Reprints and permission information is available online at <http://www.nature.com/reprints>. Correspondence and requests for materials should be addressed to H.L.A. or P.H.B.

## Competing financial interests

The authors declare no competing financial interests.

## Graphical abstract for table of contents:

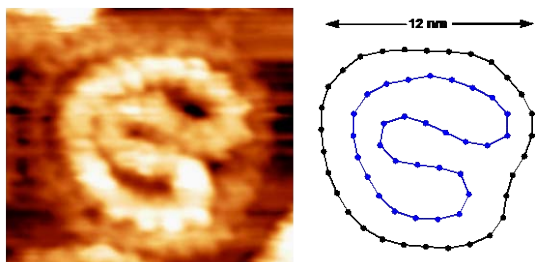


### *Table of contents summary:*

Biolpolymers achieve functional tertiary structures through folding and multiplex formation. Here we show that synthetic molecules with protein-like dimensions can exhibit biomimetic self-organisation. Monodisperse cyclic porphyrin polymers, with diameters of 13–21 nm, form nested structures on a gold surface. These assemblies are formed both under vacuum and during deposition from solution.